

Complex lithium ion dynamics in simulated LiPO_3 glass studied by means of multi-time correlation functions

Michael Vogel

Department of Chemical Engineering, University of Michigan, 2300 Hayward, Ann Arbor, MI, 48109, USA

(Dated: March 22, 2022)

Molecular dynamics simulations are performed to study the lithium jumps in LiPO_3 glass. In particular, we calculate higher-order correlation functions that probe the positions of single lithium ions at several times. Three-time correlation functions show that the non-exponential relaxation of the lithium ions results from both correlated back-and-forth jumps and the existence of dynamical heterogeneities, i.e., the presence of a broad distribution of jump rates. A quantitative analysis yields that the contribution of the dynamical heterogeneities to the non-exponential depopulation of the lithium sites increases upon cooling. Further, correlated back-and-forth jumps between neighboring sites are observed for the fast ions of the distribution, but not for the slow ions and, hence, the back-jump probability depends on the dynamical state. Four-time correlation functions indicate that an exchange between fast and slow ions takes place on the timescale of the jumps themselves, i.e., the dynamical heterogeneities are short-lived. Hence, sites featuring fast and slow lithium dynamics, respectively, are intimately mixed. In addition, a backward correlation beyond the first neighbor shell for highly mobile ions and the presence of long-range dynamical heterogeneities suggest that fast ion migration occurs along preferential pathways in the glassy matrix. In the melt, we find no evidence for correlated back-and-forth motions and dynamical heterogeneities on the length scale of the next-neighbor distance.

PACS numbers: 66.30.Dn

I. INTRODUCTION

In view of numerous technological applications and a large variety of phenomena, recent scientific work repeatedly focused on glassy ion conductors. On the one hand, it is well known that the macroscopic charge transport in these materials results from the diffusion of mobile ions in a basically rigid glassy matrix, on the other, a detailed microscopic picture of this dynamical process is still lacking. One key feature of the dynamics in glassy ion conductors is the non-exponential relaxation of the mobile ions, indicating the complexity of the motion. For instance, broad loss peaks are found in dielectrical and mechanical relaxation experiments^{1,2,3,4,5}. Moreover, when the dynamics of the mobile ions are studied by means of advanced nuclear magnetic resonance (NMR) techniques, non-exponential correlation functions are observed^{6,7,8,9}. In general, the origin of non-exponential relaxation can be twofold¹⁰. In the homogeneous scenario, the dynamics of all particles are characterized by the same relaxation function that is intrinsically non-exponential due to a specific mechanism of the motion, e.g., correlated back-and-forth jumps. Contrarily, in the heterogeneous scenario, all particles relax exponentially, i.e., there are no correlated back-and-forth jumps, but a distribution of correlation times $G(\lg \tau)$ exists. In our case of a complex motion, one may expect that both homogeneous and heterogeneous dynamics contribute to the non-exponential relaxation.

A strong frequency dependence of the electrical conductivity $\sigma(\omega)$ of ion conductors indicates that back-and-forth motions occur during ionic diffusion^{11,12,13,14,15,16,17}. However, to study a complex

motion in detail, it is not sufficient to probe the dynamics at two times, but one has to resort to multi-time correlation functions¹⁰. For example, three-time correlation functions can be used to quantify the extent to which the non-exponential relaxation results from the homogeneous and the heterogeneous scenario, respectively¹⁸. Four-time correlation functions allow one to measure the lifetime of dynamical heterogeneities, i.e., the timescale of exchange processes between fast and slow ions. Two methods have recently proven well suited to record multi-time correlation functions for glassy ion conductors. While ion dynamics on the ps–ns timescale can be studied in molecular dynamics (MD) simulations¹⁹, multi-dimensional NMR techniques probe jumps on a timescale of ms–s. Specifically, multi-dimensional ¹⁰⁹Ag NMR experiments showed that a broad rate distribution governs the jumps of silver ions in silver phosphate based glasses⁷. Hence, both correlated back-and-forth jumps and dynamical heterogeneities indeed contribute to the non-exponentiality. However, to the best of our knowledge the relevance of both contributions has not yet been quantified for glassy ion conductors.

MD simulations are an ideal tool to investigate dynamical processes on a microscopic level. Prior work on the origin of the non-exponential relaxation in glassy ion conductors has focused on alkali silicate glasses. For lithium silicate glasses, it was reported that dynamical heterogeneities contribute to the non-exponential relaxation of the lithium ions where the lifetime of these heterogeneities is limited^{19,20}. Further, back-and-forth motions on various length scales were observed, including a backward correlation beyond the first neighbor shell at low temperatures¹⁹. For sodium silicate glasses, no evidence for back-and-forth jumps between adjacent sodium

sites was found at higher temperatures²¹. Moreover, several workers demonstrated that, though there is no micro-segregation, the sodium ions follow preferential pathways in the glassy matrix^{22,23}. The sodium ions inside these channels show a higher mobility than the ones outside and, hence, dynamical heterogeneities exist²⁴. In addition, studying examples of ionic trajectories the mechanism of alkali ion migration in silicate glasses was described as "vacancy-like process"²⁵. During a correlated motion of two cations, an alkali site is left by one ion and occupied by another.

In the present work, we use MD simulations to analyze the complex mechanism of ion dynamics in an alkali phosphate glass. In this way, we intend to complement the prior studies on silicate glasses and to compare the nature of ion diffusion in different amorphous materials. Moreover, based on an analysis of novel higher-order correlation functions, new information about this dynamical process is revealed. In detail, the dynamics of non-crystalline LiPO_3 is investigated in a temperature range where the motions of the various atomic species strongly decouple upon cooling. While the lithium ionic subsystem can be equilibrated at all chosen temperatures, the diffusion of the phosphorus and the oxygen particles freezes in on the ns-timescale of the simulation. In other words, the dynamics in the melt and in the glass are studied. Our main goal is to identify the temperature dependent origin of the non-exponential relaxation of the lithium ions. For this purpose, we calculate multi-time correlation functions that link the positions of single ions at subsequent points in time. In this way, we quantify the homogeneous and the heterogeneous contributions to the non-exponential relaxation and measure the lifetime of the dynamical heterogeneities. Since the multi-time correlation functions observed in NMR experiments on solid ion conductors and some of the quantities computed in the present study have a similar information content, a future comparison of the respective results is very promising.

II. DETAILS OF THE SIMULATION

The potential used to describe the interaction of the ions in LiPO_3 can be written as the sum of a Coulomb and a Born-Mayer-Huggins pair potential

$$\Phi_{\alpha\beta}(r) = \frac{q_\alpha q_\beta e^2}{r} + A_{\alpha\beta} \exp(-r/\rho) \quad (1)$$

where r is the distance between two ions of type α and type β , respectively. The potential parameters, except for A_{LiO} , are adopted from the work of Karthikeyan et al.²⁶. Here, A_{LiO} is reduced to obtain a more realistic interatomic distance r_{LiO} , cf. below. In detail, we use effective charges $q_{\text{Li}} = 0.6$, $q_{\text{P}} = 3.0$ and $q_{\text{O}} = -1.2$ as well as $\rho = 0.29\text{\AA}$. The parameters $A_{\alpha\beta}$ are listed in Tab. 1. Most simulations are performed in the NEV ensemble

TABLE I: Interaction parameters $A_{\alpha\beta}$, cf. Eq. 1, together with the interatomic distances $r_{\alpha\beta}$ as obtained from the present simulations and from experimental work^{27,30}, respectively.

| | $A_{\alpha\beta}$ [eV] | $r_{\alpha\beta}$ [\AA] simulation | $r_{\alpha\beta}$ [\AA] experiment |
|------|------------------------|--|--|
| LiLi | 167.47 | 2.74 | |
| LiP | 158.09 | 3.31 | |
| LiO | 300.00 | 2.03 | 2.02 |
| PP | 148.93 | 3.33 | 3.01 |
| PO | 694.66 | 1.51/1.66 | 1.52–1.56 |
| OO | 2644.8 | 2.58 | 2.52 |

for $N = 800$ particles. To take into account the thermal expansion of phosphate glasses, the density is fixed at $\rho = 2.15\text{ g/cm}^3$ as compared to $\rho = 2.25\text{ g/cm}^3$ observed in experiments at room temperature²⁷. This approximation for the density at higher temperatures is obtained based on the linear expansion coefficient of LiPO_3 glass²⁸. In addition, we consider systems with $N = 200$ and $N = 400$ to check for finite size effects. Moreover, some simulations are performed at "constant pressure" to enable a comparison with experimentally determined activation energies. Strictly speaking, we continue doing runs in the NEV ensemble, but the size of the simulation box is adjusted so that a pressure $p = 7.0 \pm 0.1\text{ GPa}$ is obtained at all temperatures. This procedure results in a decrease of the density from $\rho = 2.21\text{ g/cm}^3$ at 744K to $\rho = 1.95\text{ g/cm}^3$ at 3000K. The equations of motion are integrated using the velocity form of the Verlet algorithm with a time step of 2fs. Further, periodic boundary conditions are applied and the Coulombic forces are calculated via Ewald summation. In doing so, consistent results are obtained when computing the trajectories with the programme MOLDY²⁹ and an own MD simulation programme, respectively. While the whole system can be equilibrated at $T \geq 1006\text{K}$, the phosphate glass matrix is basically frozen on the timescale of the simulation at lower temperatures. In the latter cases, we pay attention that the lithium ionic subsystem is still in equilibrium. For example, the sample is equilibrated for 20ns at $T = 592\text{K}$ before recording the data.

Karthikeyan et al.²⁶ demonstrated that the structure of LiPO_3 glass is well reproduced when using the two-body potential specified in Eq. 1. We confirmed this result by analyzing the structure of the glass obtained after a quench from $T = 592\text{K}$ to $T = 300\text{K}$. Tab. 1 shows that the interatomic distances $r_{\alpha\beta}$ are in good agreement with the corresponding experimental values^{27,30}. Typical of phosphate glasses³¹, the P-O distance for bridging oxygens ($r_{\text{PTO}} = 1.51\text{\AA}$) is shorter than for bridging oxygens ($r_{\text{PBO}} = 1.66\text{\AA}$). Further, the reduction of A_{LiO} , as compared to the value used by Karthikeyan et al.²⁶, improves the agreement with the actual distance r_{LiO} ^{27,30}. Consistent with experimental findings for LiPO_3 glass^{31,32,33}, the bond-angle distributions and the coordination num-

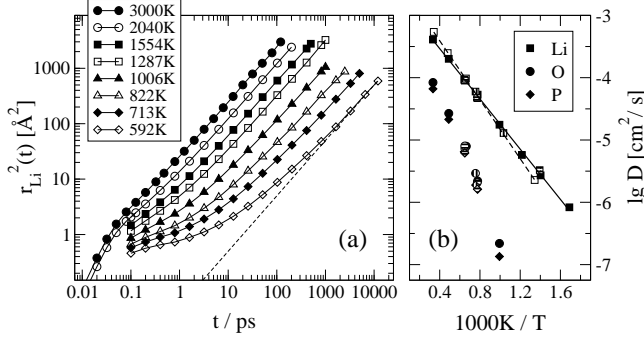


FIG. 1: (a): MSD of the lithium ions, $r_{Li}^2(t)$, in non-crystalline $LiPO_3$ at the indicated temperatures. Dashed line: $r_{Li}^2(t) = 6D_{Li}t$ with $D_{Li} = 8.31 \cdot 10^{-7} \text{ cm}^2/\text{s}$. (b): Temperature dependence of the diffusion constants D_{Li} , D_O and D_P ; solid symbols: $N = 800$, $\rho = 2.15 \text{ g/cm}^3$, open symbols: $N = 800$, $p = 7.0 \text{ GPa}$, vertical stripes: $N = 400$, $\rho = 2.15 \text{ g/cm}^3$, horizontal stripes: $N = 200$, $\rho = 2.15 \text{ g/cm}^3$, lines: Arrhenius fits to the data for $N = 800$.

bers indicate that the simulated glass consists of well defined phosphate tetrahedra that are connected by two of their corners to form long chains and/or rings. Concerning the intermediate range order, some differences between simulated and actual $LiPO_3$ glass may exist. In agreement with results by Karthikeyan et al.²⁶, we find a mean P-O-P bond angle that is smaller than the one observed in experiments on vitreous P_2O_5 ³¹. To fix this mean angle at the experimental value for vitreous P_2O_5 , Liang et al.³⁴ used a three-body potential in simulations of $LiPO_3$ glass. We refrain from doing so because, first, the P-O-P bond angle in meta-phosphate glasses has not yet been determined experimentally and, second, three-body interactions distinctly slow down the simulation. For our analysis, it is important to perform simulations at sufficiently low temperatures, because not until then lithium dynamics show several characteristic features, e.g., back-and-forth jumps between adjacent sites^{19,35}. Therefore, we keep the potential as simple as possible so as to be able to equilibrate the system at these temperatures.

III. RESULTS

To study the dynamics of non-crystalline $LiPO_3$, we first display the mean square displacement (MSD) of the lithium ions

$$r_{Li}^2(t) = \langle [r^j(t)]^2 \rangle = \langle [|\vec{r}^j(t_0+t) - \vec{r}^j(t_0)|]^2 \rangle \quad (2)$$

in Fig. 1(a). Throughout this article, the brackets $\langle \dots \rangle$ denote the average over the lithium ionic subsystem, $r^j(t)$ is the displacement of lithium ion j during a time interval t and $\vec{r}^j(t_0)$ specifies its position at the time t_0 . At temperatures $T \leq 2040 \text{ K}$, $r_{Li}^2(t)$ exhibits three characteristic time regimes: ballistic motion $r_{Li}^2 \propto t^2$ at short times

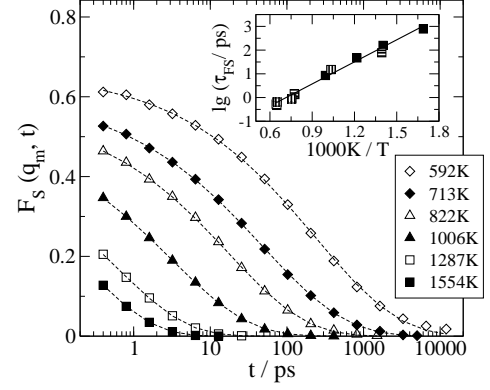


FIG. 2: Incoherent intermediate scattering function $F_s(q_m = 2.28 \text{ \AA}^{-1}, t)$ for the lithium ions in non-crystalline $LiPO_3$ at the indicated temperatures ($N = 800$, $\rho = 2.15 \text{ g/cm}^3$). Inset: Temperature dependence of the mean correlation time τ_{FS} ; solid symbols: $N = 800$, vertical stripes $N = 400$, horizontal stripes: $N = 200$, line: Fit to an Arrhenius law for $N = 800$.

$t < 0.1 \text{ ps}$, sublinear diffusion due to back-and-forth motions of the lithium ions at intermediate times and linear diffusion $r_{Li}^2 \propto t$ at long times. Upon cooling the diffusion of the lithium ions slows down and the time window of sublinear diffusion is extended. A qualitatively similar behavior is found for the MSD of the oxygen and the phosphorus ions, $r_O^2(t)$ and $r_P^2(t)$ (not shown).

The diffusion constants $D_{Li,O,P}$ extracted from the long-time behavior of $r_{Li,O,P}^2(t)$ are compiled in Fig. 1(b). Evidently, the lithium diffusion decouples from the oxygen and the phosphorus dynamics. While D_{Li} follows an Arrhenius law with activation energy $E_D = 0.40 \text{ eV}$, the curves $\lg D_{O,P}(1/T)$ show a downward bending. In particular, on the 10ns-timescale of our simulation, a basically rigid phosphate glass matrix exists below $T \approx 1000 \text{ K}$. Therefore, we refer to $T_g = 1000 \text{ K}$ as the computer glass transition of $LiPO_3$. For comparison, the diffusion constants resulting from the calculations for $N = 200$ and $N = 400$ and from the constant pressure simulations are also included in Fig. 1(b). We find no indication that the diffusion constants depend on the system size. On the other hand, the temperature dependence of D_{Li} in the constant pressure runs ($E_D = 0.47 \text{ eV}$) is stronger than in the constant volume simulations.

Next, the incoherent intermediate scattering function $F_s(q, t)$ for the lithium ions is considered:

$$F_s(q, t) = \langle \cos [\vec{q}(\vec{r}^j(t_0+t) - \vec{r}^j(t_0))] \rangle. \quad (3)$$

In our case of an isotropic sample, this function only depends on the absolute value, q , of the wave vector. To obtain information about dynamical processes on the length scale of the Li-Li interatomic distance, $q = q_m = 2\pi/r_{LiLi}$ is used. Fig. 2 shows $F_s(q_m, t)$ for the NEV ensemble ($N = 800$). We see temperature dependent, non-exponential decays. These findings can be quantified by fitting the data to a Kohlrausch-Williams-Watts (KWW)

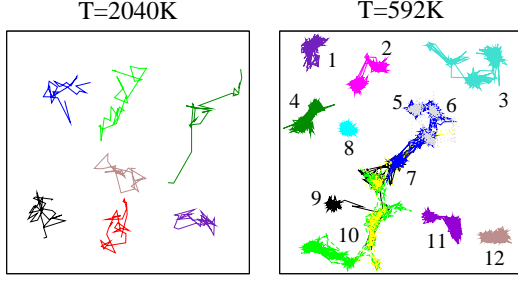


FIG. 3: Representative trajectories of the lithium ions in non-crystalline LiPO_3 . Left hand side: Trajectories at $T=2040\text{K}$ during a time interval $\Delta t=3\text{ps}$. Right hand side: Trajectories at $T=592\text{K}$ during a time interval $\Delta t=100\text{ps}$.

function³⁶, $A \exp[-(t/\tau)^\beta]$. Then, a stretching parameter $\beta \approx 0.42$ characterizes the non-exponentiality at $T < T_g$. Above T_g , an increase to $\beta \approx 0.54$ is observed, however, the absence of a short-time plateau of $F_s(q_m, t)$ leads to larger error bars in this temperature range. In the inset of Fig. 2, we display the mean time constants τ_{FS} calculated from the fit parameters according to $\tau_{FS} = (\tau/\beta)\Gamma(1/\beta)$ where $\Gamma(x)$ is the Γ -function. Though there are some deviations, the temperature dependence of τ_{FS} can still satisfactorily be described by an Arrhenius law with activation energy $E_{FS} = 0.62\text{eV}$. In the same way, $E_{FS} = 0.67 \pm 0.03\text{eV}$ is obtained from the constant pressure simulations. Thus, in both cases, E_{FS} is significantly larger than E_D . In addition, Fig. 2 shows that the time constants τ_{FS} do not depend on N and, hence, finite size effects are again absent. In the remainder of this article, we analyze the data from constant volume simulations for $N=800$.

To study the mechanism of lithium dynamics, we first look at some representative trajectories. Fig. 3 displays projections on the xy -plane for trajectories during comparable time intervals at $T=2040\text{K}$ and $T=592\text{K}$. While the mechanism of the motion resembles liquid-like diffusion at the high temperature, it is rather complex in the glass. Specifically, the following features are obvious for $T=592\text{K}$: (i) The motion of most lithium ions can be decomposed into local vibrations and jumps between adjacent sites. (ii) The lithium ions show different mobilities. (iii) Back-and-forth dynamics involve distinct lithium sites. (iv) The number of correlated back-and-forth jumps varies. While numerous back-and-forth jumps are observed for ion 4, only a few are found for ion 3. (v) Several ions (6-10) follow the same preferential pathway. Consistent with the results of simulations on alkali silicate glasses^{35,37,38,39}, all these features elucidate the complexity and the diversity of ionic diffusion in glasses.

A statistical analysis of the mechanism of the motion is possible based on the self part of the van Hove correlation

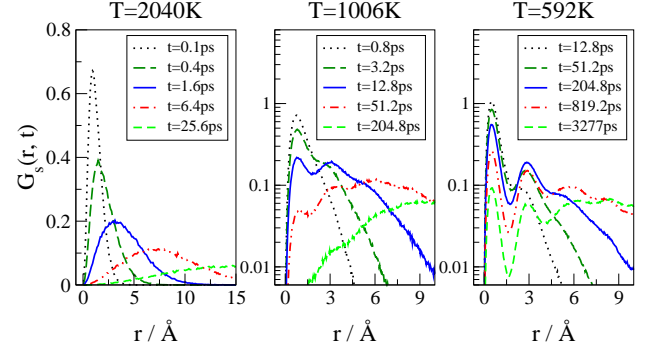


FIG. 4: Space- and time dependence of the self part of the van Hove correlation function $G_s(r, t)$ for non-crystalline LiPO_3 at the indicated temperatures.

function for the lithium ions. It is given by⁴⁰

$$G_s(r, t) = \langle \delta(r - r^j(t)) \rangle \quad (4)$$

where $\delta(x)$ denotes the δ -function. $G_s(r, t)$ measures the probability that a lithium ion moves a distance r in a time interval t . Fig. 4 shows $G_s(r, t)$ for three characteristic temperatures. For $T=2040\text{K}$, we observe a single maximum that shifts to larger values of r when t is increased. Though the findings resemble expectations for liquid-like diffusion, an asymmetry of the curves for $t \approx 1\text{ps}$ indicates deviations. For $T \leq T_g$, $G_s(r, t)$ exhibits oscillations that become more pronounced upon cooling. Specifically, there are minima at $r \approx 1.7\text{\AA}$ and $r \approx 4.2\text{\AA}$ together with a maximum at $r \approx 2.7\text{\AA} \approx r_{\text{LiLi}}$. Thus, the glassy network provides well defined lithium sites that are separated by energy barriers $E > k_B T$ so that, to a good approximation, the lithium ionic motion can be described as a sequence of hopping processes, i.e., the timescale it takes to cross the barriers is much shorter than the timescale the ions fluctuate about the sites. In particular, it is possible to distinguish between ions that, after a time t , (i) still reside at the same site ($r^j(t) \leq 1.7\text{\AA}$), (ii) have jumped to a next-neighbor site ($1.7\text{\AA} < r^j(t) < 4.2\text{\AA}$) and (iii) have moved beyond an adjacent site ($r^j(t) \geq 4.2\text{\AA}$). These findings for $G_s(r, t)$ agree with both the appearance of the trajectories in Fig. 3 and the results of previous simulations^{19,35,39,41,42,43,44}.

Next, we define the two-time correlation function $S_2(t) = \langle s_2^j(t) \rangle$ where $s_2^j(t) = 1$ for $r^j(t) \leq 1.7\text{\AA}$ and $s_2^j(t) = 0$ otherwise. In our case of hopping motion, $S_2(t)$ measures the probability that a lithium ion is still at the initial site after a time t . Thus, it directly reflects the depopulation of the initially occupied lithium sites. In Fig. 5, we see that $S_2(t)$ decays non-exponentially. This non-exponentiality can result from correlated back-and-forth jumps between neighboring sites and/or from dynamical heterogeneities, i.e., the presence of a distribution of jump rates. Based on an appropriate three-time correlation function S_3 , both contributions will be quantified later in this article. The average time it takes for the

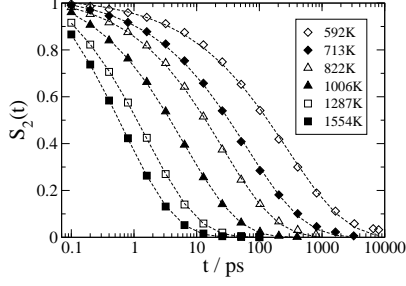


FIG. 5: Two-time correlation function $S_2(t)$ at the indicated temperatures.

lithium ions to successfully escape from their sites, i.e., the timescale of the depopulation of the sites, can be characterized by the $1/e$ -decay time of $S_2(t)$, τ_{S_2} . Fig. 6 shows that the temperature dependence of τ_{S_2} is well described by an Arrhenius law with activation energy $E_S = 0.44\text{eV}$.

In the remainder of this article, the origin of the non-exponential relaxation of the lithium ions in simulated LiPO_3 glass is studied in detail by analyzing various multi-time correlation functions. All these functions correlate the positions of single lithium ions at subsequent times $t_1 < t_2 < \dots$. To characterize the motion of ion j between two times $t_\alpha < t_\beta$, we use the notation $\vec{r}_\alpha^j \equiv \vec{r}^j(t_\alpha)$, $\vec{r}_{\alpha\beta}^j \equiv \vec{r}_\beta^j - \vec{r}_\alpha^j$, $r_{\alpha\beta}^j \equiv |\vec{r}_{\alpha\beta}^j|$ and $t_{\alpha\beta} \equiv t_\beta - t_\alpha$.

To show the existence of dynamical heterogeneities and to study their lifetime, we define a "four-time van Hove correlation function"

$$G_4(r, t_{12}=t_s, t_{23}, t_{34}=t_s) = \langle a(r_{12}) \delta(r - r_{34}^j) \rangle. \quad (5)$$

In this equation, the term $a(r_{12})$ simply means that three subensembles are selected with respect to the displacement during the time interval $t_{12} = t_s$: SE_0 consists of ions that are still at the initial site ($r^j(t_{12}) \leq 1.7\text{\AA}$), SE_1 contains the ones that have jumped to an adjacent site ($1.7\text{\AA} < r^j(t_{12}) < 4.2\text{\AA}$) and the ions of SE_2 show $r^j(t_{12}) \geq 4.2\text{\AA}$. Thus, $G_4(r, t_s, t_{23}, t_s)$ probes the

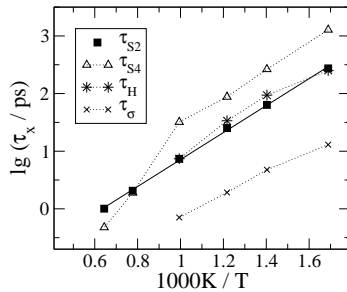


FIG. 6: Various time constants characterizing lithium ion dynamics in non-crystalline LiPO_3 , see text for details.

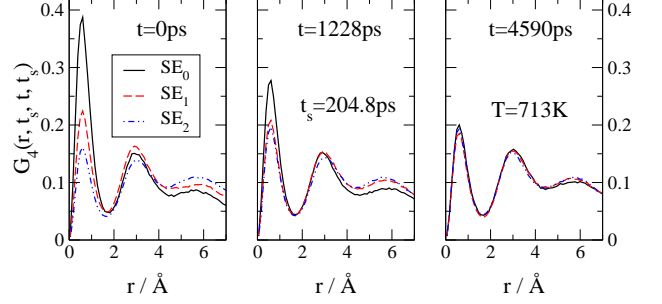


FIG. 7: Four-time van Hove correlation function $G_4(r, t_s, t, t_s)$ for the lithium ions in LiPO_3 glass at $T=713\text{K}$. A filter time $t_s=204.8\text{ps}$ was used to select three subensembles of lithium ions SE_0 , SE_1 and SE_2 , see text for details.

van Hove correlation function $G_s(r, t_s)$ of the respective subensembles starting at a time t_{23} after their selection. The results for $t_s = 204.8\text{ps}$ and various t_{23} at $T = 713\text{K}$ are displayed in Fig. 7. For $t_{23} = 0$, the three subensembles show clearly different G_4 . In particular, the first peak is highest for SE_0 , indicating that ions that have not escaped from their sites during t_{12} move also less than the average particle in the time interval t_{34} . In other words, slow and fast ions are distinguishable and, hence, dynamical heterogeneities exist¹⁰. An extension of t_{23} , i.e., of the delay between selection and detection, allows us to study the lifetime of the dynamical heterogeneities. In Fig. 7, we see that the curves for the different subensembles approach each other when t_{23} is increased until they are nearly identical after a time $t_{23} = 4.6\text{ns}$. At this time $t = 4.6\text{ns}$, the decay of $S_2(t)$ is just complete, cf. Fig. 5. Thus, the information about the initial dynamical states is lost when all ions have successfully escaped from their sites, i.e., the dynamical heterogeneities are short-lived. A more detailed analysis of the lifetime of the dynamical heterogeneities will be presented below.

For a study of back-and-forth jumps, we focus on lithium ions that have moved to a neighboring site during t_{12} and map their motion in the subsequent time interval t_{23} . This analysis is possible based on the "three-time van Hove correlation function"

$$G_3(r, t_{12}, t_{23}) = \langle d(r_{12}^j) \delta(r - r_{13}^j) \rangle \quad (6)$$

where $d(r_{12}^j) = 1$ for $1.7\text{\AA} < r_{12}^j < 4.2\text{\AA}$ and $d(r_{12}^j) = 0$ otherwise. $G_3(r, t_{12}, t_{23})$ measures $G_s(r, t = t_{12} + t_{23})$ exclusively for ions that occupy a next-neighbor site at the time t_2 . $G_3(r, t_{12}, t_{23} = 0)$ is different from zero only in the range $1.7\text{\AA} < r < 4.2\text{\AA}$. For $t_{23} > 0$, backward jumps towards the initial positions \vec{r}_1^j yield the intensity I_b at $r < 1.7\text{\AA}$, whereas forward jumps contribute to the intensity I_f at $r > 4.2\text{\AA}$. Hence, when multiple jumps are negligible, i.e., for $t_{23} < t_{12}$, the ratio I_b/I_f provides information whether the subsequent motion is backward or forward correlated. In Fig. 8, we display $G_3(r, t_{12}, t_{23})$ at $T = 592\text{K}$ for $t_{12} = 12.8\text{ps}$, 819.2ps and

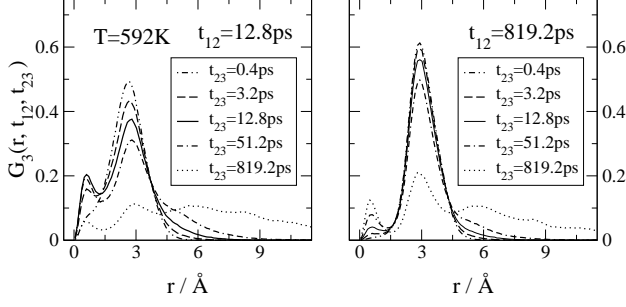


FIG. 8: Three-time van Hove correlation functions $G_3(r, t_{12}, t_{23})$ for the lithium ions in LiPO_3 glass at $T = 592\text{K}$

various t_{23} . Nearly independent of $t_{23} < t_{12}$, integration yields $I_b/I_f \approx 15$ for $t_{12} = 12.8\text{ps}$ and $I_b/I_f \approx 0.3$ for $t_{12} = 819.2\text{ps}$. While the former ratio indicates a significant backward correlation, the latter is comparable to $I_b/I_f \approx 1/3$ as expected for a random-walk based on a mean coordination number $z_{\text{LiLi}} \approx 4$. For an interpretation of these results, it is useful to recall the existence of dynamical heterogeneities and to reinspect Fig. 4. It becomes clear that the population at the neighboring site is still small after a time $t_{12} = 12.8\text{ps}$ and, hence, it mainly results from the fast ions. Vice versa, ions with a medium or a low mobility occupy an adjacent after a time $t_{12} = 819.2\text{ps}$. Hence, the curves $G_3(r, t_{12}, t_{23})$ for $t_{12} = 12.8\text{ps}$ and $t_{12} = 819.2\text{ps}$ reflect the behavior of fast and non-fast ions, respectively. We conclude that a significantly enhanced back-jump probability exists for the fast ions, but not for the slow ions.

One may argue that large-amplitude vibrations can also lead to $I_b/I_f \gg 1$ for short t_{12} . However, one expects that displacements due to vibrations are limited by $r_{12}^j < r_{\text{LiLi}}$ and, hence, a significant contribution of this type of motion would result in an asymmetry of $G_3(r, t_{12}, t_{23} \rightarrow 0)$. Therefore, the nearly symmetric shape of $G_3(r, t_{12}, t_{23} \leq 0.4\text{ps})$ shows that large-amplitude vibrations do not affect our conclusion. The finding that the back-jump probability depends on the dynamical state is backed up by preliminary results of a more detailed analysis. There, we explicitly identify the lithium sites and calculate the back-jump probability p_b as a function of the waiting time at the initial site, t_w . Consistent with results for LiSiO_2 ⁴⁵, we find that $p_b(t_w)$ significantly decreases with increasing waiting time. Thus, a high backward correlation exists exclusively for ions that show a high jump rate at the initial site.

The length scales of the dynamical heterogeneities and of the correlated back-and-forth motions can be studied based on the conditional probability functions $p(x_{23}|r_{12})$ and $p(y_{23}|r_{12})$. These functions measure the probability to find specific values $x_{23}^j = x_{23}$ and $y_{23}^j = y_{23}$, respectively, provided the particle has moved a distance $r_{12}^j = r_{12}$ in the first time interval t_{12} . Here, x_{23}^j is the

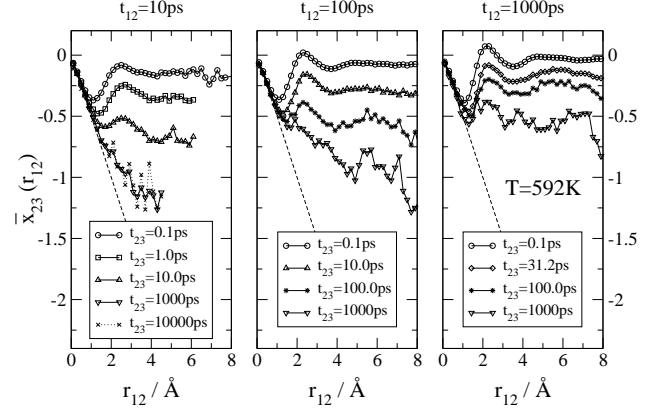


FIG. 9: First moment $\bar{x}_{23}(r_{12})$ of the conditional probability function $p(x_{23}|r_{12})$ for LiPO_3 glass at $T = 592\text{K}$. The time intervals t_{12} and t_{23} are indicated.

projection of \vec{r}_{23}^j on the direction of the motion during t_{12} , i.e., $x_{23}^j = \vec{r}_{23}^j \cdot \vec{r}_{12}^j / r_{12}^j$ and y_{23}^j is the projection of \vec{r}_{23}^j on an arbitrary direction perpendicular to \vec{r}_{12}^j . Motivated by the outcome of prior work^{19,46,47}, we focus on the first moment \bar{x}_{23} as well as on the second moments $\sigma_x(r_{12}) = \langle [x_{23}^j - \bar{x}_{23}(r_{12})]^2 (r_{12}^j) \rangle$ and $\sigma_y(r_{12}) = \langle [y_{23}^j - \bar{y}_{23}(r_{12})]^2 (r_{12}^j) \rangle$, rather than analyzing the full probability functions.

For the first moment, $\bar{x}_{23}(r_{12}) \equiv 0$ will result if the directions of the motions during t_{12} and t_{23} are uncorrelated^{46,47}. In contrast, if the subsequent motion for a given r_{12} is backward (forward) correlated, a negative (positive) value of $\bar{x}_{23}(r_{12})$ will be observed. In particular, it has been readily shown that $\bar{x}_{23}(r_{12}) = -(1/2)r_{12}$ is found for stochastic dynamics in a harmonic potential¹⁹. Fig. 9 shows $\bar{x}_{23}(r_{12})$ for $T = 592\text{K}$. For all t_{12} and t_{23} , $\bar{x}_{23}(r_{12})$ follows the curve $-(1/2)r_{12}$ up to $r_{12} = 1.0 - 1.5\text{Å}$, indicating that the lithium sites can be described by harmonic potentials on this length scale. At larger r_{12} , $\bar{x}_{23}(r_{12})$ depends on both t_{12} and t_{23} . For a given t_{12} , $\bar{x}_{23}(r_{12})$ is more negative the larger the value of t_{23} until a saturation is reached at $t_{23} \approx 1000\text{ps}$. This can be understood as follows: No significant motion occurs during short time intervals t_{23} so that $x_{23}^j \approx 0$. However, when t_{23} is extended, more and more lithium ions show a distinct displacement until the average behavior of all ions with a given r_{12} is observed for long t_{23} . To study this average behavior we further discuss the results for a long $t_{23} = 1000\text{ps}$. In this case, $\bar{x}_{23}(r_{12})$ is basically constant at $r_{12} > 1\text{Å}$ for $t_{12} = 1000\text{ps}$, whereas, for $t_{12} \leq 100\text{ps}$, a decrease over the whole accessible r_{12} range indicates that the backward correlation increases even beyond the interatomic distance r_{LiLi} . A comparison with Fig. 4 shows that, for $t_{12} \leq 100\text{ps}$, the findings in the range $r_{\text{LiLi}} \leq r_{12} < 8\text{Å}$, say, reflect the behavior of fast ions, while an ion with an average mobility shows such displacements during a time interval $t_{12} = 1000\text{ps}$. Thus, the decrease of $\bar{x}_{23}(r_{12})$ at $r_{12} \geq r_{\text{LiLi}}$ for short

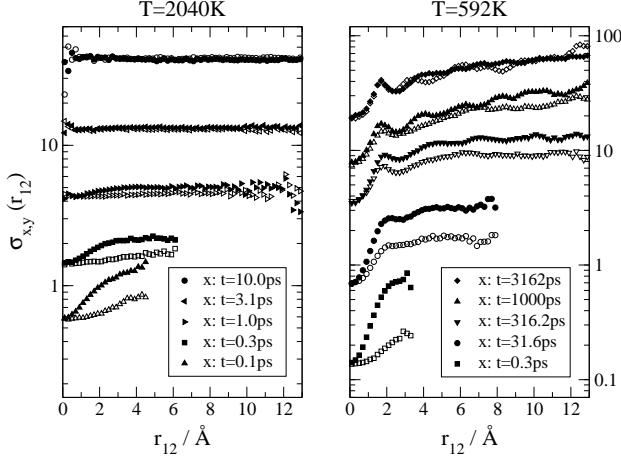


FIG. 10: Second moments $\sigma_x(r_{12})$ (solid symbols) and $\sigma_y(r_{12})$ (open symbols) of the conditional probability functions $p(x_{23}|r_{12})$ and $p(y_{23}|r_{12})$, respectively. Data for non-crystalline LiPO_3 at $T=2040\text{K}$ and $T=592\text{K}$ are compared. The time intervals $t=t_{12}=t_{23}$ are indicated.

t_{12} implies that the correlated back-and-forth motions of fast ions may involve not only one, but also several sites. On the other hand, $\bar{x}_{23} \approx \text{const.}$ at $r_{12} > 1\text{\AA}$ for long t_{12} again shows that the non-fast ions perform local rattling motions, but no correlated back-and-forth jumps between adjacent sites. We add that $\bar{x}_{23} \approx -0.24r_{12}$ at $r_{12} < 2\text{\AA}$ and $\bar{x}_{23} = \text{const.}$ at $r_{12} > 2\text{\AA}$ are found for LiPO_3 melt at $T=2040\text{K}$ ($t_{12} < 1\text{ps}$, $t_{23} \geq 1\text{ps}$). Qualitatively, these findings resemble the outcome of MD simulations on supercooled liquids^{46,47}. There, the results were interpreted as a signature of the cage effect describing that, though all particles are mobile, every particle is temporarily captured in a cage built up by its neighbors. Then, back-and-forth motions take place within the cage, but not when the particles have left their cages.

Now, we turn to the second moments. If all particles have equal mobility, the displacements r_{12} and r_{23} are uncorrelated so that $\sigma_{x,y}(r_{12}) = \text{const.}$. In contrast, if dynamical heterogeneities exist, on average, slow and fast ions show small and large r_{12} , respectively. Hence, ions with small r_{12} move less in t_{23} than those with large r_{12} and $\sigma_{x,y}(r_{12})$ increases. Fig. 10 shows $\sigma_x(r_{12})$ and $\sigma_y(r_{12})$ for various time intervals $t=t_{12}=t_{23}$ at two temperatures. For $T=2040\text{K}$, the second moments are equal and independent of r_{12} for $t > 1\text{ps}$, indicating the absence of dynamical heterogeneities related to lithium diffusion. In contrast, $\sigma_x(r_{12})$ and $\sigma_y(r_{12})$ for $t \leq 1\text{ps}$ increase, though, with a different slope and, thus there are highly anisotropic dynamical heterogeneities on short timescales. Since $r_{Li}(t < 1\text{ps}) < r_{LiLi}$, cf. Fig. 1, we attribute the latter dynamical heterogeneities to the rattling motions within the local cages. For $T=592\text{K}$, a strong r_{12} dependence of $\sigma_{x,y}$ is observed for all chosen t . This finding again implies the existence of dynamical heterogeneities attributed to lithium diffusion in the glass.

Since back jumps during t_{23} result in $x_{23}^j \neq 0$ and $y_{23} \approx 0$, i.e., the component perpendicular to the direction of the forward jump is small, the dynamical heterogeneities can be most directly studied based on $\sigma_y(r_{12})$. The ratio $\sigma_y(r_{LiLi})/\sigma_y(0) \gg 1$ shows that the heterogeneity results for the most part from different jump rates at neighboring lithium sites. However, additional contributions on a length scale of several Li-Li interatomic distances are indicated by a further increase of $\sigma_y(r_{12})$ up to $r_{12} \approx 13\text{\AA}$ for $t \geq 1000\text{ps}$. Considering also the appearance of the lithium trajectories in Fig. 3, we suggest that preferred pathways of ion migration connect several lithium sites.

The oscillatory behavior of $\bar{x}_{23}(r_{12})$ and $\sigma_{x,y}(r_{12})$ allows us to study the energy landscape governing the lithium dynamics. For $\bar{x}_{23}(r_{12})$, one expects local minima (maxima) near positions where the slope of the potential shows maxima (minima)¹⁹. In Fig. 9, we see that $\bar{x}_{23}(r_{12})$ shows a minimum at $r_{12} \approx 1.1\text{\AA}$ and a maximum at $r_{12} \approx 2.3\text{\AA}$. Hence, there should be an energy barrier at an average distance $r \approx 1.7\text{\AA}$. At $r_{12} \approx 1.7\text{\AA}$, the curves $\sigma_{x,y}(r_{12})$ exhibit local maxima. This is reasonable, because ions residing at a saddle after t_{12} should possess a comparatively high mobility in the subsequent time interval. A closer inspection of the data reveals that the maxima of $\sigma_{x,y}(r_{12})$ shift to smaller r_{12} when t is extended. As will be discussed later in this article, this finding is consistent with the assumption that the Li-Li interaction depends on the waiting time at a site.

To quantify the homogeneous and the heterogeneous contributions to the non-exponential relaxation of the lithium ions we define the three-time correlation function

$$S_3(t_{12}=t/2, t_{23}=t/2) = \langle s_2^j(t_{12})s_2^j(t_{23}) \rangle. \quad (7)$$

For purely homogeneous and purely heterogeneous relaxation, such three-time correlation functions can be expressed by the corresponding two-time correlation functions^{18,46,48,49}. While $S_3(t/2, t/2) = [S_2(t/2)]^2$ is valid in the homogeneous scenario, $S_3(t/2, t/2) = S_2(t)$ holds in the heterogeneous scenario, cf. Appendix A. In Fig. 11, $S_3(t/2, t/2)$ is shown for three temperatures. For $T=1287\text{K}$, $S_3(t/2, t/2) \approx [S_2(t/2)]^2$ implies that the relaxation is basically homogeneous. However, above T_g , hopping dynamics is not a good approximation for the mechanism of the motion and the phosphate matrix dynamics modifies the lithium sites. Therefore, our findings do not indicate back-and-forth jumps between adjacent lithium sites, but rather they reflect back-and-forth motions that are affected by the matrix dynamics and take place on various length scales. At $T < T_g$, $S_3(t/2, t/2)$ clearly deviates from $[S_2(t/2)]^2$ and, hence, dynamical heterogeneities become increasingly important upon cooling. Their relevance can be further analyzed based on the ratio

$$H(t) = \frac{S_3(t/2, t/2) - [S_2(t/2)]^2}{S_2(t) - [S_2(t/2)]^2}. \quad (8)$$

It is easily seen that $H(t) \equiv 1$ and $H(t) \equiv 0$ hold for

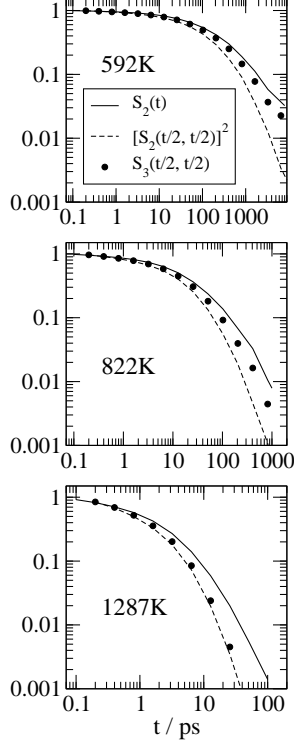


FIG. 11: Three-time correlation functions $S_3(t/2, t/2)$ for non-crystalline LiPO_3 at the indicated temperatures. The results are compared to the expectations for purely heterogeneous dynamics, $S_2(t)$, and for purely homogeneous dynamics, $[S_2(t/2)]^2$.

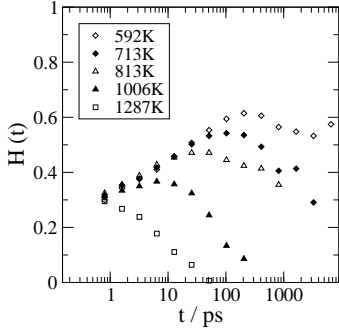


FIG. 12: $H(t)$ for non-crystalline LiPO_3 at the indicated temperatures. The data were calculated from the results in Fig. 11 using Eq. 8.

purely heterogeneous and purely homogeneous dynamics, respectively. In Fig. 12, $H(t)$ is displayed for the studied temperatures. Evidently, the non-exponentiality at low temperatures results to a large extent from dynamical heterogeneities, i.e., there is a broad distribution of jump rates. For $T \leq 1006\text{K}$, the curves $H(t)$ show

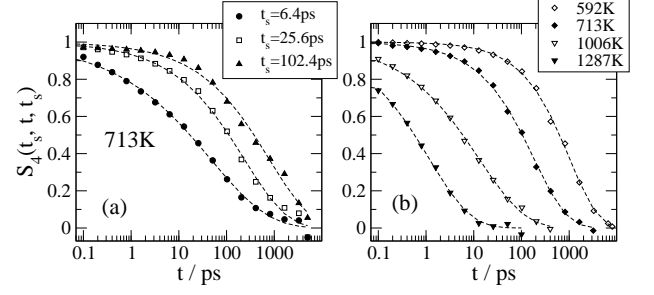


FIG. 13: Four-time correlation functions $S_4(t_s, t, t_s)$ for non-crystalline LiPO_3 (points) and fits to a KWW function (dashed lines). (a): Data at $T = 713\text{K}$ for the indicated filter times t_s . (b): Temperature dependence of the curves for comparable filter times, i.e., $S_2(t_s) = 0.48 \pm 0.02$ (592K: $t_s = 145.0\text{ps}$, 713K: $t_s = 40.0\text{ps}$, 1006K: $t_s = 4.0\text{ps}$, 1287K: $t_s = 1.2\text{ps}$).

a maximum at a time τ_H that increases upon cooling. Inspecting the temperature dependence of τ_H in Fig. 6, $\tau_H(T) \approx \tau_{S_2}(T)$ is found. Thus, the distribution of jump rates contributes most to the non-exponentiality when the lithium ions successfully escape from their sites.

The lifetime of the dynamical heterogeneities can be measured based on the four-time correlation function

$$S_4(t_{12}=t_s, t, t_{34}=t_s) = \langle s_2^j(t_{12}) s_2^j(t_{34}) \rangle. \quad (9)$$

In this experiment, a dynamical filter selecting lithium ions that are slow on the timescale t_s^{50} is applied during two time intervals $t_{12} = t_s$ and $t_{34} = t_s$ separated by a time t . Thus, $S_4(t_s, t, t_s)$ is given by the fraction of lithium ions that are slow during t_{12} and a time t later during t_{34} . Consequently, the signal decreases when slow ions become fast in the time interval t and mapping $S_4(t)$ allows us to measure the timescale of the exchange of the dynamical state. In Fig. 13, various normalized correlation functions $S_4^n(t)$ are compiled. In panel (a), we show results for different filter times t_s at $T = 713\text{K}$ and, in panel (b), we display data for comparable t_s at various temperatures ($S_2(t_s) \approx 0.48$). For the normalization, $S_4(t)$ was fitted to a modified KWW function, $\Delta S_4 \exp[-(t/\tau)^\beta] + S_4^\infty$, and scaled according to $S_4^n(t) = (S_4(t) - S_4^\infty)/\Delta S_4$. Evidently, $S_4^n(t)$ depends on both the filter time and the temperature where all decays are non-exponential. The non-exponentiality indicates that the exchange processes between slow and fast ions cannot be described by a single time constant, but are rather governed by a broad distribution of exchange times. Further, since dynamically diverse subensembles are selected for different filter times t_s , the dependence on this parameter implies that the exchange time depends on the dynamical state itself. A comparison with Fig. 5 reveals that the decays of $S_2(t)$ and $S_4(t)$ are complete at comparable times. In accordance with the interpretation of G_4 , this finding shows that the information about the initial dynamical states is lost when all lithium ions have successfully escaped from their sites. The mean

time constants τ_{S4} , i.e., the mean exchange times, can be calculated from the parameters of the KWW fits to $S_4(t)$. Revisiting Fig. 6 we see that τ_{S4} and τ_{S2} show a similar temperature dependence at $T \leq T_g$. All these findings consistently indicate that the exchange of the dynamical state in the glass results from successful jumps among neighboring lithium sites. Above T_g , a stronger temperature dependence of τ_{S4} is observed. Hence, the modification of the lithium sites due to matrix dynamics provides another channel for the exchange of the dynamical state in the melt.

IV. DISCUSSION

In this article, we presented MD simulations performed to study the dynamics of non-crystalline LiPO_3 in a temperature range where the motions of the various atomic species strongly decouple, i.e., the dynamics in the melt ($T > T_g$) and in the glass ($T < T_g$) were compared. We found that the mechanism of the lithium motion changes from liquid-like diffusion to hopping dynamics when the temperature is decreased. Our main goal was to study the lithium ionic jumps at $T < T_g$. Non-exponential two-time correlation functions, such as the incoherent intermediate scattering function, and sublinear diffusion over several orders of magnitude in time reflect the complexity of the lithium motion in a rigid phosphate glass matrix. For a comprehensive analysis of this dynamical process, we calculated suitable multi-time correlation functions. Three time-correlation functions showed that the non-exponential relaxation of the lithium ions at $T < T_g$ results from both correlated back-and-forth jumps and the existence of dynamical heterogeneities, i.e., the presence of a distribution of jump rates. Measuring the lifetime of the dynamical heterogeneities by means of four-time correlation functions, we found that the non-uniformities of the motion are short-lived. In what follows, we summarize and discuss our results in more detail where the quantities that lead to the respective conclusion are indicated in brackets.

The dynamical heterogeneities at $T < T_g$ show the following features: (i) The distribution of jump rates contributes more to the non-exponentiality the lower the temperature (S_3 , H). (ii) For a given temperature, its contribution is maximum when the lithium ions successfully escape from their sites (τ_H/τ_{S2}). (iii) The exchange between the fast and the slow ions of the distribution takes place on the same timescale as the lithium jumps, i.e., the dynamical heterogeneities are short-lived (G_4 , S_4). In particular, both processes show a similar temperature dependence (τ_{S4}/τ_{S2}). (iv) The timescale of the exchange depends on the dynamical state itself (S_4). (v) The dynamical heterogeneities mainly result from different jump rates at neighboring sites, but there are also non-uniformities of the motion on a length scale $r \geq 10\text{\AA}$ ($\sigma_{x,y}$). The back-and-forth jumps of the lithium ions in the glass can be characterized as follows: (i) Correlated

back-and-forth jumps occur for the fast ions of the distribution, but not for the slow ions, i.e., the back-jump probability depends on the initial dynamical state (G_3 , \bar{x}_{23}). (ii) For highly mobile ions, there is a backward correlation even beyond the first neighbor shell (\bar{x}_{23}). Well above T_g , dynamical heterogeneities and back-and-forth motions on the length scale r_{LiLi} are absent (\bar{x}_{23} , $\sigma_{x,y}$). However, due to the temporary caging of the lithium ions by the neighboring particles, anisotropic dynamical heterogeneities and a backward correlation exist on short length- and timescales.

We conclude that the formation of well-defined lithium sites is accompanied by the emergence of correlated back-and-forth jumps and dynamical heterogeneities on a length scale $r \geq r_{LiLi}$. At the lower temperatures, the non-exponential depopulation of the lithium sites results to a large extent from the dynamical heterogeneities and, hence, the distribution of jump rates is broad. The short lifetime of the dynamical heterogeneities implies that sites featuring fast and slow lithium dynamics, respectively, are intimately mixed. In particular, the absence of long-lived heterogeneities excludes a micro-segregation of the glass into extended clusters in which the lithium ions are mobile and immobile, respectively. Instead, we suggest that the broad distribution of jump rates in LiPO_3 glass results from a diversity of the local glass structure at neighboring sites, e.g., from varying coordination numbers. In this basically random energy landscape, fast ion migration occurs along pathways connecting low energy barriers. The presence of such channels is not only indicated by the appearance of the lithium trajectories, but also by the existence of long-range dynamical heterogeneities and by the backward correlation beyond the first neighbor shell for the fast ions.

Some of our findings are recovered when analyzing the dynamics resulting from schematic models such as the random-barrier and the random-energy model where the particles move in a time-independent, external energy landscape. For example, the particles migrate along preferential pathways in these models and percolation approaches have been applied to describe the dynamics at low temperatures^{51,52,53}. Moreover, the back-jump probability depends on the dynamical state of a particle, e.g., for the random-barrier model, many back-and-forth jumps occur over low energy barriers, whereas slow ions cross high barriers so that a backward motion is unlikely. However, other features of the lithium dynamics in LiPO_3 glass are not reproduced in schematic models. At variance with our findings, cf. Fig. 12, a straightforward calculation shows that $H(t \rightarrow 0) \approx 0.5$ is obtained for these models. Furthermore, we observe that the first maximum of $\sigma_{x,y}(r_{12})$ lies at $r > r_{LiLi}/2$ and shifts towards shorter distances when t is increased, cf. Fig. 10. This means that, in contrast to what is captured in simple models, the energy barriers crossed by the fast lithium ions of the distribution are located at larger distances than the ones overcome by the slow ions. We speculate that simple hopping models are suited to study the time-

independent effects of the glassy matrix on the lithium ionic diffusion, but they fail in modelling the influence of the time-dependent Li-Li interactions. For example, we want to demonstrate that our findings for the position of the energy barrier can be explained when assuming that the Li-Li interaction decreases with the waiting t_w at a site due to the adjustment of the neighboring lithium ions. For simplicity, we consider a lithium ion that occupies a site at $r = 0$ and experiences a potential $V(r, t_w) = -\cos(\pi r) + (1/2)a(t_w)r^2$. Here, the first and the second term are meant to mimic the contribution from the glassy matrix and from the repulsion due to other lithium ions ($a(t_w) \geq 0$), respectively. A Taylor expansion for $r \approx 1$ shows that the maximum of this potential lies at $r_m(t_w) = 1/(1 - a(t_w)/\pi^2)$. Hence, for $da(t_w)/dt_w < 0$, this simple model yields a maximum at $r_m(t_w) \geq 1$ that is located at smaller distances the larger the value of the waiting time as observed in our simulations.

Comparing the results of MD simulation studies on phosphate and silicate glasses several similar features of cation dynamics are striking: (i) It is widely accepted that cation diffusion at sufficiently low temperatures can be described as a sequence of hopping processes^{19,35,39,41,42,43,44}. (ii) $F_s(q_m, t)$ consistently shows non-exponential decays that are well described by KWW functions with stretching parameters $\beta = 0.42 - 0.47$ ^{23,35}. (iii) Dynamical heterogeneities with a limited lifetime exist²⁰ that become more pronounced when the temperature is decreased¹⁹. (iv) Fast ion transport along preferential pathways takes place^{22,24}. (v) A high back-jump probability exists for the fast ions of the distribution, but not for the slow ions⁴⁵. On the other hand, in previous work on sodium silicate glasses²¹, correlated back-and-forth jumps were not observed at somewhat higher temperatures. However, since, a high back-jump probability exists only for the fast ions at sufficiently low temperatures, the percentage of ions showing correlated back-and-forth jumps may have been too small to be detected in the study by Sunyer et al.²¹. Altogether, though it is to be further clarified to which extent the findings of MD simulations reflect the dynamics in a specific system at lower temperatures, the similarity of the simulation results for various interaction potentials suggests that the mechanism of cation dynamics in various glassy ion conductors is highly comparable.

Finally, we compare our results with experimental findings. First, it can be noted that two-time correlation functions of lithium dynamics obtained in experiments and simulations for LiPO₃ glass show a similar non-exponentiality. Specifically, the stretching parameter $\beta \approx 0.42$ found here compares well to $\beta = 0.33 - 0.54$ observed in electrical and mechanical relaxation studies^{3,4,5,12} and in multi-dimensional ⁷Li NMR experiments⁵⁴. Further, in these measurements, an activation energy $E_a \approx 0.68$ eV was obtained for the lithium dynamics. Comparing this value with the results of our constant pressure simulations good agreement is found for $E_{FS} \approx 0.67$ eV, but sig-

nificant differences must be noted for $E_D = 0.47$ eV. For the moment, it is not clear where the difference between E_{FS} and E_D results from. Since similar deviations were reported in MD simulation studies of LiSiO₂ glass¹⁹, one may speculate that they are a consequence of the complexity of ion dynamics in glasses.

In addition, our findings are useful for the interpretation of experimental results on the origin of the non-exponential relaxation of the mobile ions in solid ion conductors. Multi-dimensional ¹⁰⁹Ag NMR experiments on glassy and crystalline silver ion conductors^{7,55} showed that the non-exponential silver ionic relaxation is due to the existence of a broad distribution of jump rates rather than to correlated back-and-forth jumps. On the other hand, the presence of correlated back-and-forth motion is indicated by a frequency dependence of the electrical conductivity $\sigma(\omega)$ ^{11,12,13,14,15,16,17}. We suggest that this apparent discrepancy can be cleared up based on the present results. Specifically, we found that, first, the back-jump probability depends on the dynamical state, see also⁴⁵, and, second, the contribution of the dynamical heterogeneities to the non-exponentiality increases upon cooling. Since $\sigma(\omega)$ is dominated by the fast ions, we expect a disproportional contribution from the correlated back-and-forth jumps of ions in this dynamical state. In contrast, multi-dimensional NMR experiments probe the behavior of non-fast ions at low temperatures and, hence, if at all, back-and-forth jumps should be of minor relevance.

In summary, various techniques have to be applied simultaneously to obtain a complete picture of a complex dynamical process such as ion dynamics in solids. In particular, a further comparison of results obtained in MD simulations and in multi-dimensional NMR experiments is very promising since both techniques allow one to study a dynamical process on a microscopic level. For such a comparison, the multi-time correlation functions S_2 , S_3 and S_4 can be particularly useful, because their information content is similar to the one of the corresponding quantities in NMR experiments.

Acknowledgments

The author thanks S. C. Glotzer, A. Heuer and J. Kieffer for a generous grant of computer time and many stimulating discussions. Funding by the Deutsche Forschungsgemeinschaft (DFG) in the frame of the Emmy-Noether Programm is gratefully acknowledged.

APPENDIX A: CALCULATION OF THREE-TIME CORRELATION FUNCTIONS

It is well established for supercooled liquids that, for purely homogeneous and purely heterogeneous relaxation, three-time correlation functions comparable to S_3 can be expressed by the corresponding two-time corre-

lation functions^{18,46,48,49}. Here, $S_3(t/2, t/2) = [S_2(t/2)]^2$ follows, because no selection is possible for purely homogeneous dynamics. Hence, the dynamics during t_{12} and t_{23} , respectively, are statistically independent so that the joint probability for an escape in neither time interval can be written as a product. If this was not true a dynamically diverse subensemble could be selected based on the motion in the first time interval and, thus, dynamical heterogeneities would exist. For purely heterogeneous dynamics, the correlation functions result from a superposition of the contributions of exponentially relaxing subensembles. For the subensemble characterized by a correlation time τ_i , one has

$$S_{2,i}(t) = \exp\left(-\frac{t/2 + t/2}{\tau_i}\right) = S_{2,i}(t/2)S_{2,i}(t/2)$$

$$= S_{3,i}(t/2, t/2).$$

The second equals sign is due to the definition of the exponential function, and the third results, because the relation for purely homogeneous dynamics holds for the exponentially relaxing, undecomposable subensembles. Since $S_{3,i}(t/2, t/2) = S_{2,i}(t)$ is valid for all subensembles, $S_3(t/2, t/2) = S_2(t)$ follows.

-
- ¹ C. T. Moynihan, L. P. Boesch and E. L. Laberge, *Phys. Chem. Glasses* 14, 122 (1973)
 - ² C. Liu and C. A. Angell, *J. Non-Cryst. Solids* 83, 162 (1986)
 - ³ D. L. Sidebottom, P. F. Green and K. L. Brow, *J. Non-Cryst. Solids* 183, 151 (1995)
 - ⁴ P. F. Green, D. L. Sidebottom, R. K. Brow and J. J. Hudgens, *J. Non-Cryst. Solids* 231, 89 (1998)
 - ⁵ P. F. Green, E. F. Brown and R. K. Brow, *J. Non-Cryst. Solids* 255, 87 (1999)
 - ⁶ M. Vogel, C. Brinkmann, A. Heuer and H. Eckert, *J. Non-Cryst. Solids* 307-310, 971 (2002)
 - ⁷ M. Vogel, C. Brinkmann, A. Heuer and H. Eckert, *Phys. Chem. Chem. Phys.* 4, 3237 (2002)
 - ⁸ M. Vogel, C. Brinkmann, A. Heuer and H. Eckert, *Solid State Nuclear Magn. Reson.* 22, 344 (2002)
 - ⁹ F. Qi and R. Böhmer, *Solid State Nucl. Magn. Reson.* 22, 484 (2002)
 - ¹⁰ R. Böhmer, R. V. Chamberlin, G. Diezemann, B. Geil, A. Heuer, G. Hinze, S. C. Kuebler, R. Richert, B. Schiener, H. Sillescu, H. W. Spiess, U. Tracht and M. Wilhelm, *J. Non-Cryst. Solids* 235-237, 1 (1998)
 - ¹¹ A. K. Jonscher, *Nature* 267, 673 (1977)
 - ¹² S. W. Martin and C. A. Angell, *J. Non-Cryst. Solids* 83, 185 (1986)
 - ¹³ M. D. Ingram, *Phys. Chem. Glasses* 28, 215 (1987)
 - ¹⁴ S. R. Elliot, *Sol. State Ionics* 70/71, 27 (1994)
 - ¹⁵ K. L. Ngai, *J. Non-Cryst. Solids* 203, 232 (1996)
 - ¹⁶ K. Funke and C. Cramer, *Curr. Opin. Solid State Mater. Sci.* 2, 483 (1997)
 - ¹⁷ B. Roling, A. Happe, K. Funke and M. D. Ingram, *Phys. Rev. Lett.* 78, 2160 (1997)
 - ¹⁸ A. Heuer and K. Okun, *J. Chem. Phys.* 106, 6176 (1997)
 - ¹⁹ A. Heuer, M. Kunow, M. Vogel and R. D. Banhatti, *Phys. Rev. B.* 66, 224201 (2002)
 - ²⁰ J. Habasaki and Y. Hiwatari, *Phys. Rev. E* 65, 021604 (2002)
 - ²¹ E. Sunyer, W. Kob and P. Jund, *J. Non-Cryst. Solids*, 307-310, 939 (2002)
 - ²² P. Jund, W. Kob and R. Jullien, *Phys. Rev. B* 64, 134303 (2001)
 - ²³ J. Horbach, W. Kob and K. Binder, *Phys. Rev. Lett.* 88, 125502 (2002)
 - ²⁴ E. Sunyer, P. Jund and R. Jullien, *Phys. Rev. B* 65, 214203 (2002)
 - ²⁵ A. N. Cormack, J. Du and T. R. Zeitler, *Phys. Chem. Chem. Phys.* 4, 3193 (2002)
 - ²⁶ A. Karthikeyan, P. Vinatier, A. Levasseur and K. J. Rao, *J. Phys. Chem. B* 103, 6185 (1999)
 - ²⁷ K. Muruganandam, M. Seshasayee and S. Patanaik, *Sol. St. Ionics* 89, 313 (1996)
 - ²⁸ S. English and W. E. S. Turner, *J. Am. Ceram. Soc.* 13, 182 (1930)
 - ²⁹ K. Refson, *Comput. Phys. Commun.* 126, 310 (2000)
 - ³⁰ S. Beaufils, M. Bionducci, C. Ecolivet, R. Marchand and A. Le Sauze, *Sol. St. Commun.* 116, 687 (2000)
 - ³¹ U. Hoppe, G. Walter, R. Kranold and D. Stachel, *J. Non-Cryst. Sol.* 263-264, 29 (2000) and references therein
 - ³² R. K. Brow, *J. Non-Cryst. Sol.* 263-264, 1 (2000) and references therein
 - ³³ Leo van Wüllen, H. Eckert and G. Schwering, *Chem. Mater.* 12, 1840 (2000)
 - ³⁴ J.-J. Liang, R. T. Cygan and T. M. Alam, *J. Non-Cryst. Solids* 263-264, 167 (2000)
 - ³⁵ A. Heuer, M. Kunow, M. Vogel and R. D. Banhatti, *Phys. Chem. Chem. Phys.* 4, 3185 (2002)
 - ³⁶ R. Kohlrausch, *Pogg. Ann. Phys.* 4, 56 (1854); G. Williams and D.C. Watts, *Trans. Faraday Soc.* 66, 80 (1970)
 - ³⁷ M. A. Manalang, D. B. Bergstrom, D. E. Kramer and J. Kieffer, *J. Non-Cryst. Solids* 169, 72 (1999)
 - ³⁸ J. Kieffer, *J. Non-Cryst. Solids*, 172-174, 1285 (1994)
 - ³⁹ W. Smith, G. N. Greaves and M. J. Gillan, *J. Chem. Phys.* 103, 1995 (1995)
 - ⁴⁰ J. P. Hansen, I. R. McDonald, *Theory of Simple Liquids*, Academic Press, London (1986)
 - ⁴¹ S. Balasubramanian, K. J. Rao, *J. Phys. Chem.* 98, 10871 (1994)
 - ⁴² J. Habasaki, *J. Non-Cryst. Solids* 12, 183 (1995)
 - ⁴³ B. Park and A. N. Cormack, *J. Non-Cryst. Solids* 255, 112 (1999)
 - ⁴⁴ J. Horbach, W. Kob and K. Binder, *Chem. Geology* 174, 87 (2001)
 - ⁴⁵ H. Lammert, M. Kunow and A. Heuer, submitted to *Phys. Rev. Lett.*
 - ⁴⁶ B. Doliwa and A. Heuer, *Phys. Rev. Lett.* 80, 4915 (1998)
 - ⁴⁷ J. Quian, R. Hentschke and A. Heuer, *J. Chem. Phys.* 110,

- 4514 (1999)
- ⁴⁸ A. Heuer, U. Tracht, S. C. Kuebler and H. W. Spiess, J. Molec. Structure 479, 251 (1999)
- ⁴⁹ U. Tracht, PhD thesis, University of Mainz, Germany (1998)
- ⁵⁰ Strictly speaking, the dynamical filter selects lithium ions that are at the same site at the beginning and at the end of the filter time t_s .
- ⁵¹ J. C. Dyre and T. B. Schroder, Rev. Mod. Phys. 72, 873 (2000)
- ⁵² S. D. Baranovskii and H. Cordes, J. Chem. Phys. 111, 7546 (1999)
- ⁵³ B. I. Shklovskii and A. L. Efros, Electronic Properties of Doped Semiconductors, Springer Verlag, Heidelberg(1984)
- ⁵⁴ M. Vogel, C. Brinkmann, A. Heuer and H. Eckert (unpublished results)
- ⁵⁵ M. Vogel, C. Brinkmann, A. Heuer and H. Eckert, submitted to Phys. Rev. Lett.